Using a tuned fluid inerter for improving the seismic performance of structures isolated with friction pendulum system

Dario De Domenico[1], Giuseppe Ricciardi[2]
[1] *Department of Engineering, University of Messina, Italy, dario.dedomenico@unime.it*
[2] *Department of Engineering, University of Messina, Italy, gricciardi@unime.it*

Abstract: The fluid inerter is the hydraulic realization of the inerter. It consists of a piston-cylinder device that conveys a fluid through an external helical channel, thereby generating rotational inertia of a fluid mass. Unlike other variants of the inerter (e.g. ball screw, rack-and-pinion inerter, and inerter with clutch), the assumption of linear behavior for the fluid inerter is largely inaccurate, because this device is characterized by a marked nonlinear damping effect. While identification and modeling of the fluid inerter were discussed in the relevant literature, the effect of its nonlinear damping contribution in relationship to structural vibration control remains unclear. Aim of this contribution is to present a feasibility study in which the nonlinear damping contribution of the fluid inerter is examined numerically. Some experimental findings relevant to a small-scale prototype of fluid inerter justify the assumption of nonlinear power law damping, in parallel with linear inertance. The fluid inerter is here employed in combination with low-damping rubber isolators as linear restoring terms, thus realizing a novel control scheme called Tuned Fluid Inerter (TFI). In this paper, the TFI is adopted to improve the seismic performance of isolated buildings. Optimal parameters of the fluid inerter are determined using random vibration theory, by modeling the base acceleration as a zero-mean Kanai-Tajimi stationary random process, and resorting to statistical linearization to handle the nonlinear terms. The seismic performance of structures equipped with friction pendulum system (FPS) is comparatively analyzed considering a classical Tuned Mass Damper (TMD), the Tuned Mass Damper Inerter (TMDI) with mechanical inerter, and the novel TFI. Based on a benchmark six-story building, the seismic performance of the various structural control systems is analyzed in terms of isolators' displacement demand, interstory drift and acceleration response. It is shown that the effect of the inherent nonlinear damping of the fluid inerter is crucial for reducing the peak response under pulse-like ground motions that may occur in near-field earthquake events.

Keywords: Tuned Mass Damper, Fluid Inerter, Inerter, Nonlinear damping, Passive vibration control, Optimal design, Seismic base isolation, Friction pendulum isolators.

1. Introduction

The inerter is a relatively new mechanical device capable to develop a resisting force proportional to the relative acceleration of its two terminals. The constant of proportionality, called inertance, has dimensions of mass and is called inertance. The inerter device completes the force-current analogy between mechanical and electrical networks, besides the spring and the dashpot elements. Since its introduction in 2002 (Smith, 2002), the inerter has been studied and applied to different fields. Of particular relevance to the present contribution, the inerter has totally revolutionized the technology of vibration control because of its inherent capability to adjust the inertial properties of a system without allocating actual physical mass (Ikago et al., 2012). Just to quote a few prominent examples, inerter-based systems were used to improve the

performance of tuned mass dampers (TMDs), by partly or totally replacing the tuned mass thus realizing a lightweight and cost-effective device called Tuned Mass Damper Inerter (TMDI) (Giaralis and Taflanidis, 2018; Pietrosanti et al. 2017) and Tuned Inerter Damper (TID) (Lazar et al., 2014; Gonzalez-Buelga et al., 2017), respectively. Inerters were also studied to realize nonlinear energy sinks (Javidialesaadi and Wierschem, 2019), for vibration mitigation of cables (Lazar et al., 2016), for wind-vibration control of high-rise buildings (Giaralis and Petrini, 2017; Wang et al., 2019), for seismic protection of buildings (Takewaki et al., 2012; Zhao et al., 2019) and storage tanks (Luo et al., 2016; Jiang et al., 2020), or in combination with traditional base isolation systems (De Domenico and Ricciardi 2018b, 2018c; Hashimoto et al., 2015; Di Matteo et al. 2019). Focusing on the latter field of application, in seismic base isolation the dis-placement demand is mostly concentrated at the level of the isolation devices, which should be flexible enough to shift the fundamental frequency of the structure to a low-frequency (high-period) region, where the energy transferred by the ground-motion base acceleration is typically low. While the isolators guarantee low base shear and structural accelerations in the superstructure, flexible isolation devices imply large displacement demands as a counter effect. These displacements can be of the order of 40-70 cm depending on the earthquake intensity and on the selected flexibility characteristics of the isolators. Moreover, base-isolated structures may suffer from undesired resonance effects under near-field long-period ground motions (Takewaki et al., 2011). Hence, various strategies have been proposed to reduce isolators' dis-placements, such as providing supplemental damping, using adaptive energy dissipation systems like gap dampers combined with isolators (Zargar et al., 2013; De Domenico et al. 2020a), or through hybrid control strategies combining base isolation with a TMD located above or below the isolation level (Taniguchi et al., 2008; De Domenico and Ricciardi 2018a). In this regard, the effectiveness and robustness of the TMD in mitigating isolators' displacement is closely related to the mass actually allocated, which may be hampered by feasibility considerations and architectural constraints. This is why the use of inerter-based vibration absorbers turns out to be particularly useful to reduce the displacements of isolators without employing large mass ratios.

Along this research line, an inerter-based vibration absorber is proposed in this paper to improve the seismic performance of base-isolated structures equipped with Friction Pendulum System (FPS). Unlike most of the literature studies that studied the performance of the inerter in its various mechanical configurations, e.g. rack-and-pinion inerter, ball screw inerter or inerter with clutch (Málaga-Chuquitaype et al., 2019), the present contribution addresses the hydraulic realization of the device, called *fluid inerter* (Swift et al., 2013). A peculiarity of the fluid inerter is related to its marked nonlinear damping effect, whose effect in the vibration control of structures is still unclear (Smith and Wagg, 2016). Therefore, the proposed study aims at investigating a novel Tuned Fluid Inerter (TFI) system for applications to base-isolated buildings, in particular, to buildings equipped with FPS. Optimal design of the fluid inerter parameters is conducted using random vibration theory, with the base acceleration being modeled as a stationary Kanai-Tajimi zero-mean Gaussian random process. The nonlinearities of FPS and fluid inerter are handled through statistical linearization. Seismic performance of the proposed system is finally analyzed considering a series of ground motion records having different frequency characteristics. The effect of the inherent nonlinear damping contribution of the fluid inerter is also analyzed and discussed.

2. Hysteretic properties of the helical fluid inerter

A sketch of the helical fluid inerter is shown in Figure 1. As can be seen, this device consists of a piston-cylinder block that, due to its linear movement, conveys a fluid through an external helical channel, which

generates rotational inertial of the fluid mass. Due to the rotational movement of the fluid, a main component of the resisting force is the so-called inerter contribution that is proportional to the relative acceleration of the two device terminals, and the proportionality coefficient (inertance b with dimensions of mass) is related to the volume of fluid and to the squared ratio of the cylinder area to helical channel area A_1 / A_2 (Swift et al., 2013)

$$F_{\text{inerter}} = b\ddot{x} \quad \text{with} \quad b = \frac{m_{hel}}{1+\left(h/2\pi r_4\right)^2}\left(\frac{A_1}{A_2}\right)^2 \tag{1}$$

where x denotes the linear movement of the piston (relative displacement of the two terminals of the device). In Eq. (1) $m_{hel} \approx \rho_f \ell A_2$ is the mass of the fluid in the helical channel, with ρ_f denoting the mass density of the fluid, while ℓ and $A_2 = \pi r_3^2$ represents the length and cross-sectional area of the helical channel, respectively. Based on Eq. (1), a desired value of inertance can be obtained by simply adjusting the geometrical parameters of the device for given physical properties of the fluid.

Besides the inerter force in Eq. (1), other contribution to the total resisting force are (Swift et al., 2013): 1) the damping effects due to the pressure drops caused by the viscosity of the internal fluid; 2) inlet and outlet forces at the transition from the cylinder to the helical tube and vice-versa; 3) shear friction between walls of the piston and the surrounding cylinder; 4) friction effects at the two seals at either end of the piston rod moving inside the cylinder. These four contributions have the following expressions

$$\begin{aligned}
&1)\ F_{d-\text{helical}} = c_p^{NL}\dot{x}^{1.75} \quad \text{with} \quad c_p^{NL} = \frac{0.0664\mu_f^{0.25}\rho_f^{0.75}\ell A_1}{r_3^{1.25}}\left(\frac{A_1}{A_2}\right)^{1.75} \\
&2)\ F_{d-\text{inlet}} = c_1\dot{x}^2 \ \text{ with } \ c_1 = 0.25A_1\rho_f\left(\frac{A_1}{A_2}\right)^2; \quad F_{d-\text{outlet}} = c_2\dot{x}^2 \ \text{ with } c_2 = 0.5A_1\rho_f\left(\frac{A_1}{A_2}\right)^2 \\
&3)\ F_{\text{shear}} = \frac{\mu_f 2\pi r_2 L}{\Delta r}\dot{x} \\
&4)\ F_{\text{friction}} = f_0\,\text{sgn}(\dot{x})
\end{aligned} \tag{2}$$

where μ_f is the dynamic viscosity of the fluid, Δr is the clearance between piston head and cylinder wall (typically in the order of $\Delta r = 0.1$mm (Swift et al., 2013)), and f_0 is a friction coefficient that can be calibrated from pseudo-static experimental test. Following Eqns. (1) and (2), the total resisting force of the fluid inerter is the sum of an inerter force F_{inerter} (proportional to the relative acceleration) and a total damping force (dependent on the relative velocity), the latter being the sum of all the contributions appearing in Eq. (2):

$$F = F_{\text{inerter}} + F_{\text{damping,tot}} \tag{3}$$

The influence of the various terms contributing to the total damping force is analyzed in an attempt to develop a simplified model that can be used for practical earthquake engineering purposes. In Figure 2 (left) the damping terms expressed in Eq. (2) are plotted in a semi-logarithmic scale with increasing piston velocities from 0.2 m/s to 1 m/s. The geometrical parameters of the fluid inerter are those of the patent

document (Glover et al., 2009, while the internal fluid is assumed to be water ($\rho_f = 1000\,\mathrm{kg/m^3}$, $\mu_f = 10^{-3}\,\mathrm{Pa\,s}$). It is clearly seen that, among the four damping terms, the most important contribution is the helical tube damping force, which almost coincides with the total damping force. To confirm this result, in Figure 2 (right) the force-displacement loops under a sinusoidal imposed motion having frequency 1.5 Hz e amplitude 50 mm (maximum velocity of 470 mm/s) for the complete model and for a simplified model including only the helical tube damping term are compared. As can be seen, the simplified model (whose dynamic sketch is reported in the bottom-right part of Figure 1) is accurate enough to describe the hysteretic characteristics of the fluid inerter device. As a result, for preliminary design purposes, the inlet and the outlet terms, as well as the shear forces can be practically neglected. The fluid inerter can be modeled as a linear inerter in parallel with a nonlinear dashpot (power law damping factor of 1.75).

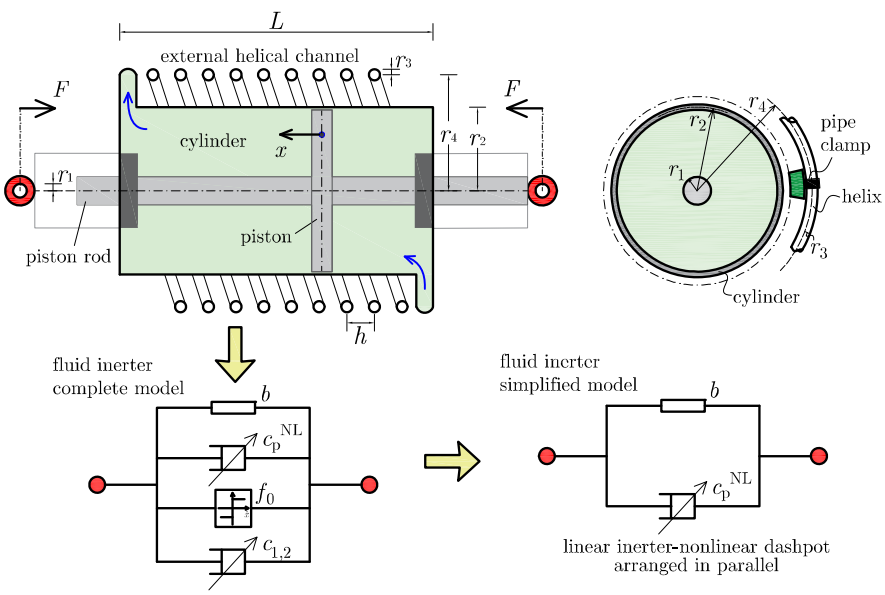

Figure 1. Helical fluid inerter (top) and related simplified mechanical models.

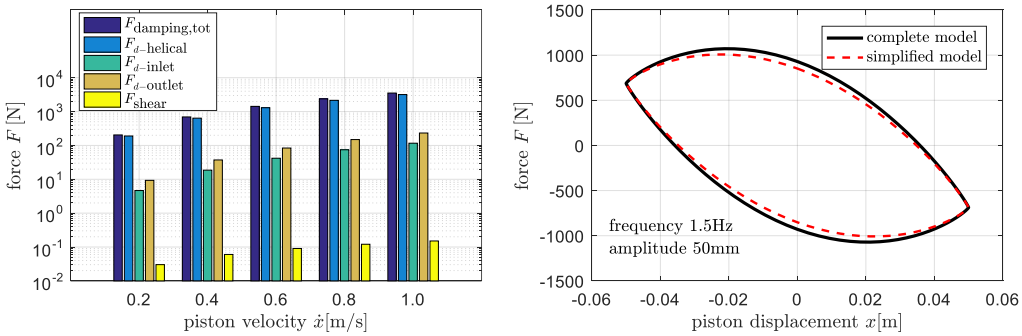

Figure 2. Contributions to the total damping force of the fluid inerter (left) and corresponding hysteretic curve un-der an imposed sinusoidal displacement.

The simplified model of a linear inerter in parallel with a nonlinear dashpot is validated against experimental results from the literature. In particular, a small-scale fluid inerter with 7 coils and filled with a silicone oil ($\rho_f = 802\,\text{kg/m}^3$ and $\mu_f = 0.00168\,\text{Pa s}$) was tested by Smith and Wagg (2016), and the corresponding experimental results (for a sinusoidal displacement amplitude of 17.5 mm and frequency 3 Hz) are shown in Figure 3, along with pertinent numerical simulations obtained by the complete and simplified model. It can be observed that the numerical models are accurate enough to capture the actual resisting force variation obtained by the experiments. Interestingly, the complete and simplified models are almost superimposed to each other, thus confirming the validity of the simplified model composed of a linear inerter in parallel with a nonlinear dashpot, which will be used afterwards in this paper.

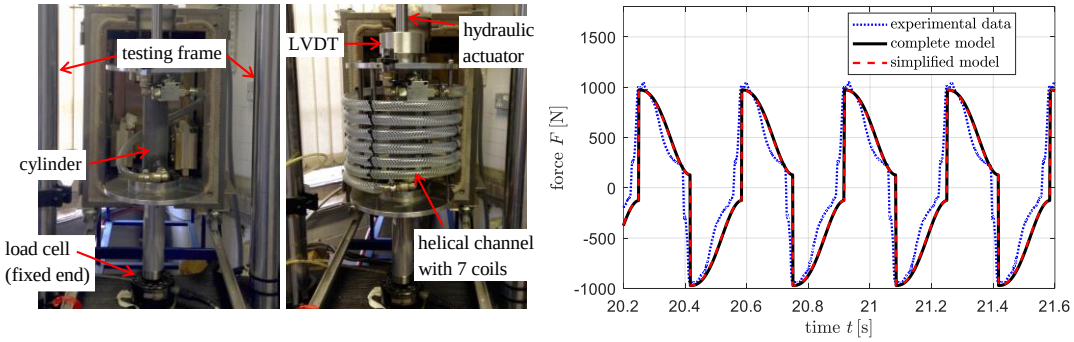

Figure 3. Laboratory tests on a small-scale fluid inerter (Smith and Wagg, 2016) and corresponding validation of the numerical model against experimental force results.

3. Building isolated with FPS equipped with tuned fluid inerter (TFI)

A simple model of *n*-story framed building isolated with FPS equipped with a tuned fluid inerter (TFI) is reported in Figure 4. The overall structure is thus composed of two systems, the primary system, i.e. the base-isolated building (with FPS), and the secondary system i.e. the TFI. In particular, the TFI is a grounded fluid inerter device that is connected to the base isolation floor through some linear restoring elements (providing the secondary system with the necessary re-centering function). Such linear restoring elements, idealized as a spring and a dashpot element arranged in parallel, can be practically realized via low-damping rubber bearings, as sketched in Figure 4. The FPS is modeled through a simplified Coulomb frictional model (rigid-plastic behavior), thus neglecting the complicated variability of the friction coefficient with axial load, sliding velocity and heating phenomena for simplicity. The equations of motion of the combined structure subjected to a horizontal earthquake-induced acceleration $\ddot{u}_\text{g}$ are expressed as follows

$$\begin{aligned} &\mathbf{M}_\text{s}\ddot{\mathbf{u}}_\text{sr} + \mathbf{C}_\text{s}\dot{\mathbf{u}}_\text{sr} + \mathbf{K}_\text{s}\mathbf{u}_\text{sr} = -\mathbf{M}_\text{s}\boldsymbol{\tau}_\text{s}\left(\ddot{u}_\text{g} + \ddot{u}_\text{b}\right) \\ &m_\text{b}\ddot{u}_\text{b} + F_{FPS} - F_{\text{s1,b}} - F_\text{rubber} = -m_\text{b}\ddot{u}_\text{g} \\ &m_\text{t}\ddot{u}_\text{t} + F_\text{rubber1} + F_\text{FI1} = -m_\text{t}\ddot{u}_\text{g} \end{aligned} \tag{4}$$

where $\mathbf{M}_\text{s}, \mathbf{C}_\text{s}, \mathbf{K}_\text{s}$ denote the mass, damping and stiffness matrices of the superstructure, respectively, $\mathbf{u}_\text{sr} = \mathbf{u}_\text{s} - \boldsymbol{\tau}_\text{s} u_\text{b}$ is the vector of superstructure displacements relative to the base-isolation floor, where,

$\mathbf{u}_s = [u_{s1},\ldots,u_{sn}]^T$ are the displacements relative to the ground, $\boldsymbol{\tau}_s$ is an n-dimensional vector of ones and u_b is the displacement of the FPS relative to the ground. Moreover, m_b indicates the mass of the base-isolation floor, $F_{FPS} = k_b u_b + f_b W_{tot}\,\mathrm{sgn}(\dot{u}_b)$ is the resisting force of the FPS, where $k_b = W_{tot}/R$ is the pendulum stiffness of the FPS (W_{tot} is the total weight of the overall structure) and f_b is the friction coefficient at the sliding interface, $\mathrm{sgn}(\cdot)$ is the signum function. Finally, $F_{s1,b} = c_1\dot{u}_{sr1} + k_1 u_{sr1}$ is the force transferred from the first floor of the superstructure to the FPS, $F_{rubber} = c_t\dot{u}_{tb} + k_t u_{tb}$ is the resisting force of the low-damping rubber bearings, dependent on relative displacements and velocities between TFI and FPS ($u_{tb} = u_t - u_b$ and $\dot{u}_{tb} = \dot{u}_t - \dot{u}_b$), and $F_{FI} = b\ddot{u}_t + c_p^{NL}\left|\dot{u}_t\right|^{1.75}\mathrm{sgn}(\dot{u}_t)$ is the nonlinear resisting force of the fluid inerter. The system of equations (4) is nonlinear due to the terms F_{FPS} and F_{FI}.

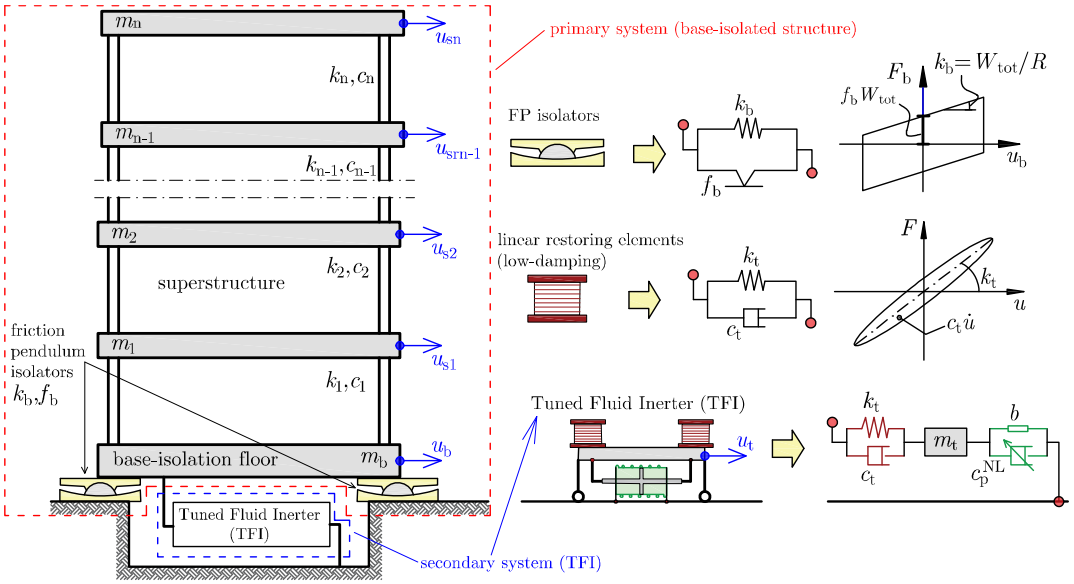

Figure 4. Model of a framed building with FPS equipped with tuned fluid inerter.

The base acceleration $\ddot{u}_g$ is modeled as a stationary zero-mean filtered Kanai-Tajimi random process, with filter parameters calibrated to capture different frequency characteristics of the earthquake excitation (De Domenico et al., 2020b)0. Moreover, the nonlinear terms F_{FPS} and F_{FI} can be linearized by resorting to the stochastic linearization technique, by converting the nonlinear contributions into linear viscous damping terms as follows

$$\begin{aligned} F_{FPS}^{SL} &= k_b u_b + c_{b,eq}\dot{u}_b \qquad \text{FPS} \\ F_{FI}^{SL} &= b\ddot{u}_t + c_{p,eq}\dot{u}_t \qquad \text{fluid inerter} \end{aligned} \tag{5}$$

where the linearization coefficients $c_{b,eq}$ and $c_{p,eq}$ can be obtained under the simplifying assumption of Gaussian response, which gives (De Domenico et al., 2019a; De Domenico et al., 2020b)

$$c_{\mathrm{b,eq}} = f_b W_{tot} \sqrt{\frac{2}{\pi}} \frac{1}{\sigma_{\dot{u}_\mathrm{b}}} \qquad \text{FPS}$$
$$c_{p,\mathrm{eq}} = 1.3952\, c_p^{NL} \sigma_{\dot{u}_\mathrm{t}}^{0.75} \qquad \text{fluid inerter} \tag{6}$$

in which $\sigma_{\dot{x}}$ denotes the standard deviation of the response process $\dot{x}$ (with $x = u_\mathrm{b}, u_\mathrm{t}$).

4. Optimal design of the fluid inerter parameters

The optimization of the fluid inerter parameters is carried out in a probabilistic framework, by assuming as objective function specific stochastic performance indices, i.e., combinations of the terms of the covariance matrices of the system response. In particular, once the linearization coefficients in Eq. (6) are defined, the linearized equations of motion can be solved in the frequency domain, so as to determine the response transfer functions and, by integration, the covariance matrices of the system response (De Domenico et al., 2020b).

In particular, the goal of the optimization procedure is to find the best inertance ratio $\beta = b / M_\mathrm{tot}$, and the best nonlinear damping ratio of the fluid inerter $\zeta_p^{NL} = c_p^{NL} / 2\sqrt{k_\mathrm{b} M_\mathrm{tot}}$ (where M_tot is the total mass of the structure) that minimize a specific objective function. The superstructure is set as a six-storey reinforced concrete building with a fundamental period $T_\mathrm{s} = 0.5\mathrm{s}$ and an inherent damping ratio of $\zeta_\mathrm{s} = 0.02$. The mass of each storey is assumed constant and equal to the mass of the base-isolation floor, so that the mass ratio $\mu_\mathrm{s} = M_{\mathrm{s,tot}} / M_\mathrm{tot} = 6/7$. A broad optimization study was discussed in a recent paper by the authors (De Domenico et al., 2020b). For the sake of brevity, in this contribution only a limited set of results are discussed. In particular, in Figure 5 we report the trend of the optimal fluid inerter parameters $\beta_\mathrm{opt}, \zeta_{p,\mathrm{opt}}^{NL}$, the corresponding linearization coefficients of both FPS and fluid inerter $\zeta_{\mathrm{b,eq}}, \zeta_{p,\mathrm{eq}}$, as well as the seismic performance of the system. The seismic performance is described in terms of four different response indicators, namely the variance of the top-storey displacement $\bar{\sigma}_\mathrm{us}^2$ (which is the objective function that is minimized in this case), the variance of the top-storey absolute acceleration $\bar{\sigma}_{\ddot{u}_\mathrm{As}}^2$, an energy-based indicator called filtered energy index (FEI) and the variance of the stroke of the TFI $\bar{\sigma}_\mathrm{utb}^2$. The FEI is a useful energy indicator quantifying the portion of input energy that is not dissipated by the passive vibration control system and, consequently, that filters into the structure. The FEI has been found to be a robust objective function for the optimization of a variety of passive vibration control systems, including hysteretic dampers, large-mass ratio TMDs (Reggio and De Angelis, 2015), TMDI (De Domenico and Ricciardi, 2018c) and viscous dampers (De Domenico et al., 2019b).

The above-mentioned response indicators are all shown in a normalized format (divided by the corresponding response indicator in the system without TFI), so that values below one indicate reduction. The results are plotted for four different earthquake frequency contents (firm, medium, soft soil and white-noise excitation as an idealization of an extremely broadband random process) in terms of the stiffness ratio $\kappa = k_\mathrm{t} / k_\mathrm{b}$. The other parameters are set as follows: $\mu_\mathrm{t} = m_\mathrm{t} / M_\mathrm{tot} = 0.005$; $f_\mathrm{b} = 0.04$; $\omega_\mathrm{b} = \sqrt{k_b / M_{tot}} = \sqrt{g / R} = \pi$; $\zeta_\mathrm{t} = c_\mathrm{t} / 2\sqrt{k_\mathrm{t} m_\mathrm{t}} = 0.1$.

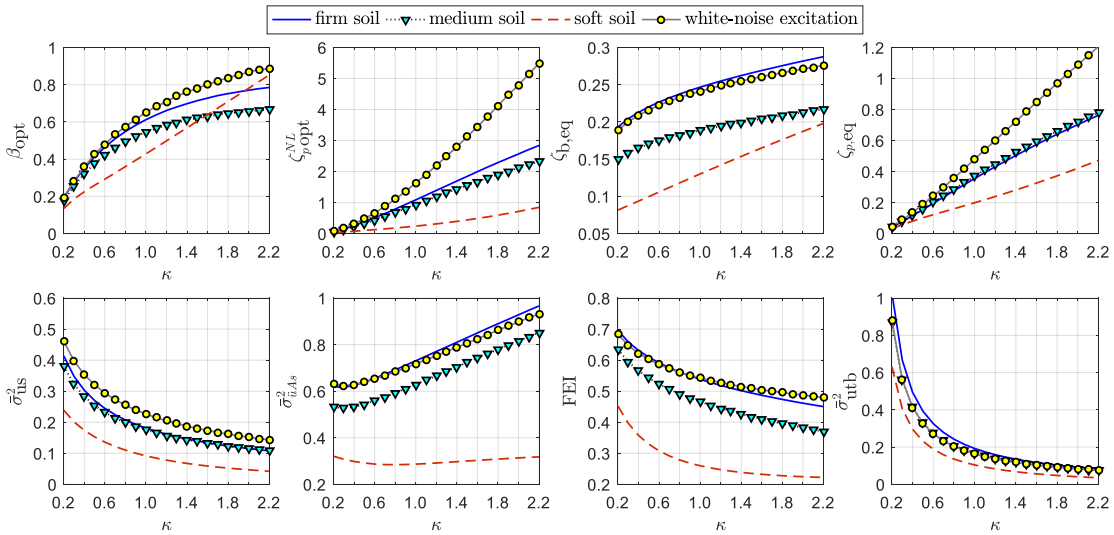

Figure 5. Optimal design and seismic performance of the FPS-TFI system for different soil conditions.

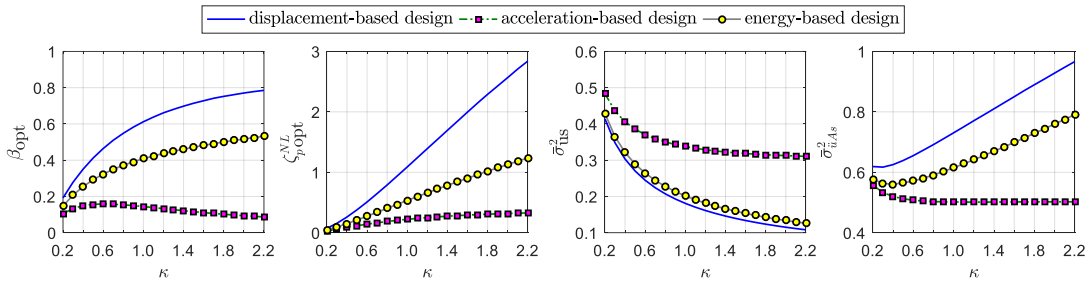

Figure 6. Optimal design and seismic performance of the FPS-TFI system for different design strategies.

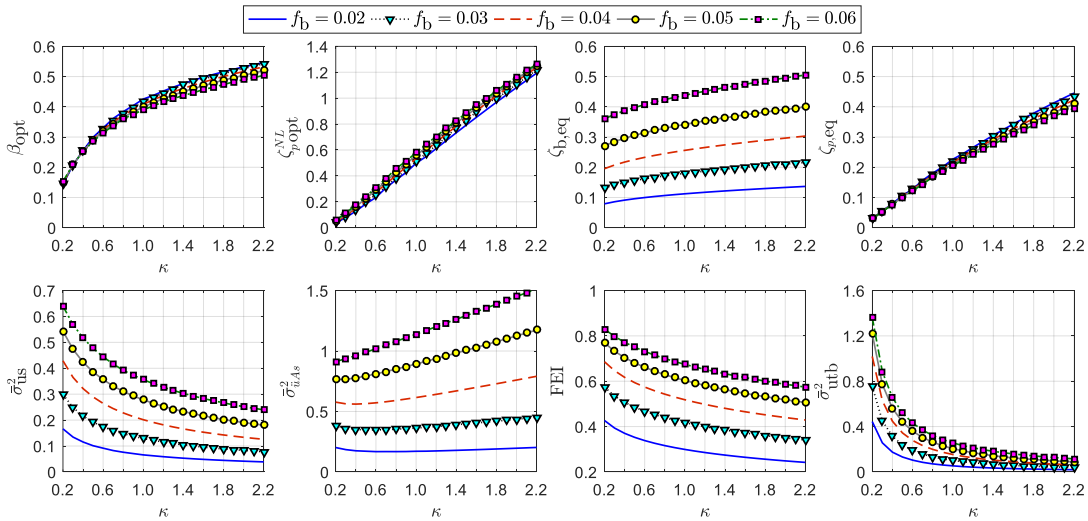

Figure 7. Optimal design and seismic performance of the FPS-TFI system for friction coefficient of the friction isolators.

Based on Figure 5, the values of β_{opt} and $\zeta_{p,\text{opt}}^{NL}$ increase with increasing κ. For the assumed parameters, the increase of the stiffness ratio κ produces a better performance in terms of displacement response, stroke of the TFI and energy dissipation, but is causes a slight increase of the absolute acceleration response. Based on the observed plots, a reasonable value for κ could be 0.8 to compromise between displacement and acceleration response. The soil conditions affect the trend of the optimal parameters: in particular, for soft soil conditions, the optimal fluid inerter parameters (both β_{opt} and $\zeta_{p,\text{opt}}^{NL}$) are lower than in the other soil conditions, at least for $\kappa < 1.4$.

The optimal fluid inerter parameters are obviously affected also by the design strategy, i.e., by the selection of the objective function to minimize. To demonstrate this, in Figure 6 the trend of the optimal design parameters along with the seismic performance in terms of displacement and absolute acceleration response are shown. Three curves are shown, each related to a specific objective function to minimize (displacement, acceleration or filtered energy index). In line with previous studies dealing with linear inerters (Pietrosanti et al., 2017; De Domenico and Ricciardi, 2018c), the energy-based design procedure (FEI) is a good compromise to obtain a reasonable reduction of both displacement and absolute acceleration. Moreover, the optimal fluid inerter parameters related to the FEI are bounded from below and from above by those obtained by the displacement- and acceleration-oriented optimal design procedures, respectively. Finally, the effect of the friction coefficient of the FPS is investigated in Figure 7, ranging from 2% to 6%. It is noted that the friction coefficient f_b has a modest influence on the optimal fluid inerter parameters, but significantly affects the control performance. In particular, higher f_b are associated with worse control performance, especially in terms of absolute acceleration response.

5. Seismic performance of FPS-TFI combined isolation system

The seismic performance of the proposed FPS-TFI combined isolation system is assessed via time history analyses considering a set of natural ground motion records. In particular, the FEMA P695 far-field (FF) and near-field (NF) record sets, comprising 44 and 56 records, respectively, are considered. Details of these records can be found in (De Domenico et al., 2020b). The records were all preliminarily scaled to have a common peak ground acceleration (PGA) of 0.3 g, so as to eliminate the randomness related to the input intensity level.

The superstructure is assumed to be a regular idealized six-storey framed building, as shown in Figure 8, with floor mass $m_f = 100000\text{kg}$ and constant lateral stiffness $k_f = 270\text{MN/m}$ equal at all storeys, which results in a fundamental period $T_{s1} \approx 0.50\text{s}$. The base-isolation system comprises 16 friction pendulum (FP) isolators. The FPS characteristics are assumed as $\omega_b = \pi$ and $f_b = 0.04$. The base-isolation floor mass is assumed equal to the floor mass, so as to obtain a total mass of $M_{tot} = 700000\,\text{kg}$. Based on the previous optimization results, a stiffness ratio $\kappa = 0.8$ is assumed, along with a damping ratio of $\zeta_t = 0.1$. The practical implementation of the TFI is realized with 4 additional low-damping rubber bearings, 4 fluid inerters and a set of bi-directional rollers, as sketched in Figure 8. The TFI is attached to the isolation floor through a rigid steel frame, located underneath the low-damping rubber bearings and able to transfer the shear force from such auxiliary isolators to the foundation through the fluid inerter. The mass of the overall rigid steel frame is $m_t = 3500\text{ kg}$, based on a reasonable set of HEB100 profiles plus transversal stiffeners.

It is worth noting that this mass is just 0.5 % of the total mass of the base-isolated structure, which corresponds to a very low mass ratio $\mu_t = 0.005$. The advantage of the mass-amplification effect induced by the fluid inerter is indeed related to the possibility of realizing lightweight vibration absorbers, thus avoiding architectural issues due to the need of allocating large masses. Based on the optimal design procedure explained in Section 4, the minimization of the objective function FEI leads to inertance ratio $\beta_{\text{opt}} = 0.341$ and damping ratio $\zeta_{p,\text{opt}}^{NL} = 0.362$.

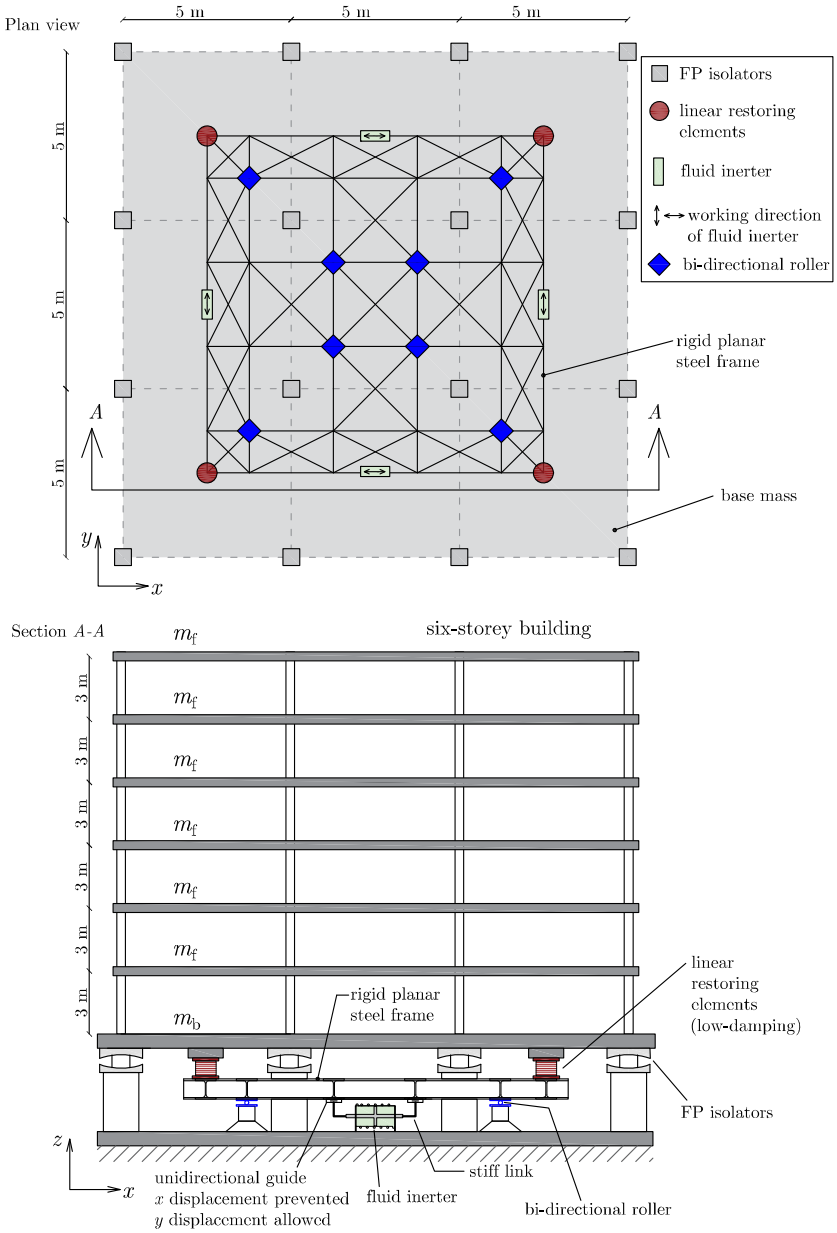

Figure 8. Six-storey framed building with proposed FPS-TFI system, plan view (top) and front view (bottom).

The seismic performance of the proposed FPS-TFI combined isolation system is compared to the classical base isolation system (FPS alone) in terms of displacements relative to the ground (normalized with respect to the top-floor displacement of the structure with FPS alone), interstory drift ratios (IDRs), assuming an interstorey height of 3.0 m, and absolute floor accelerations. To highlight the additional benefits of the combined inertance and damping properties of the fluid inerter in comparison to the classical mechanical inerter (TMDI scheme), the seismic performance of a FPS-TMDI coupled system (previously analyzed in 0) is also reported. Finally, a large-mass ratio TMD (with $\mu_t = 0.10$ in place of $\mu_t = 0.005$) coupled with the FPS is also reported in this comparative study.

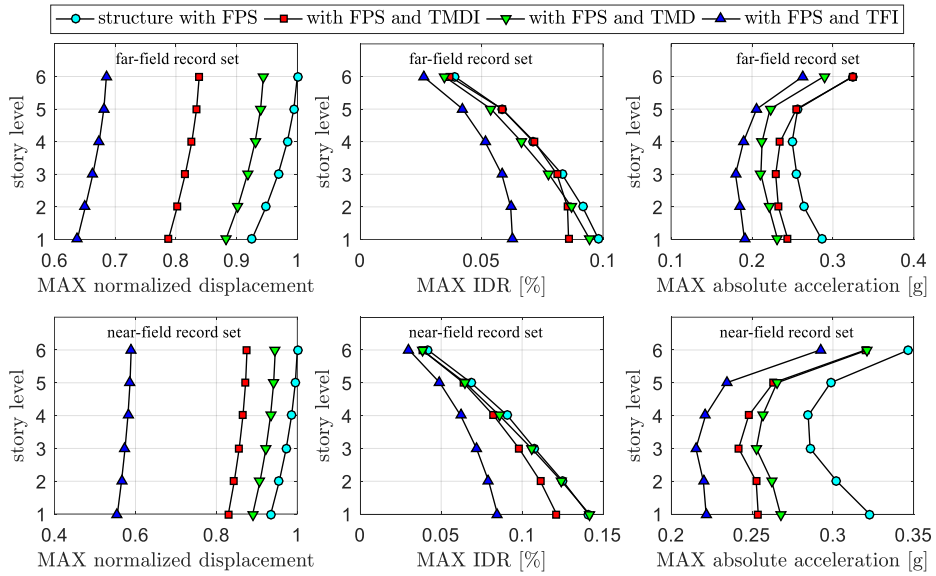

Figure 9. Average MAX displacements, interstorey drifts and absolute accelerations of benchmark structure with different structural control systems for both far-field and near-field FEMA P695 record sets.

Average maximum results (selectively considering the 44 records of the far-field set or the 56 records of the near-fault set of the FEMA P695 database) are illustrated in Figure 9. The FPS-TFI combined isolation system leads to a marked reduction of the response in comparison to the structure with FPS alone, not only of the isolators' displacements (of around 30% and 40% for FF and NF record sets, respectively), but also of the IDRs (of more than 30% for both FF and NF record sets) and of the absolute accelerations (of around 25% for both FF and NF record sets). Moreover, the FPS-TFI combined system is better able to mitigate the seismic response than the classical TMDI scheme, as well as than a large mass ratio TMD.

What is interesting to highlight is the significantly better performance of the FPS-TFI combined system under near-fault pulse-like earthquake events compared to both structure with FPS alone and structure with FPS-TMDI combined isolation system. To demonstrate this aspect, in Figure 10 the time histories of the last-floor displacement and of the last-floor absolute acceleration response under two near-fault pulse-like records, namely 1979 Imperial Valley RSN 182 and 1980 Irpinia RSN 292, are illustrated. As expected, it is noted that the strong motion phase is limited to within a very short time interval, which is typical of a pulse-like response. The inherent nonlinear damping features of the TFI are essential to mitigate the peak values

of the response in the strong motion phase, something that is not effectively achieved by the other two alternative structural control systems. In particular, the FPS-TFI system reduces the maximum displacement and the maximum absolute acceleration of around 50% and 30%, respectively, compared to the structure with FPS alone. The reduction percentages achieved by the classical TMDI scheme are, instead, relatively modest for this specific case of near-fault pulse-like events.

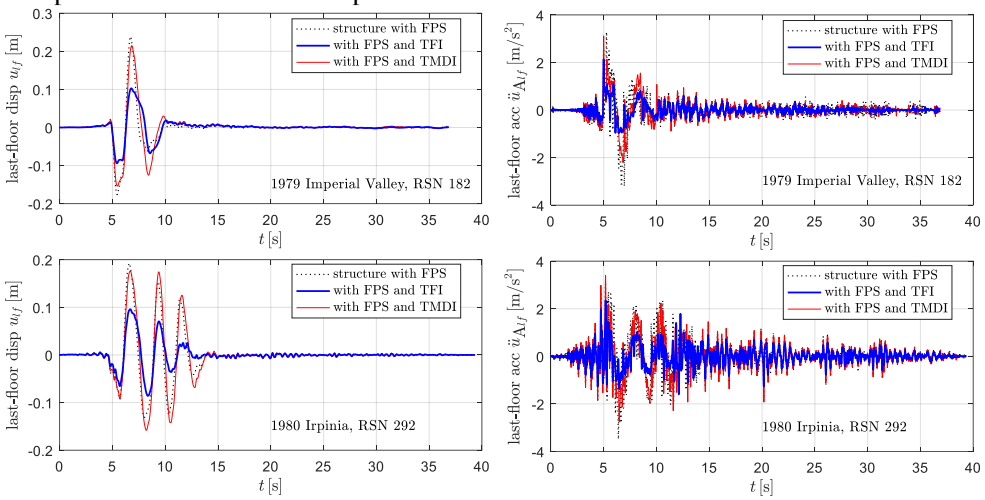

Figure 10. Last-floor displacement and absolute acceleration time histories under two near-fault pulse-like events.

6. Conclusions and critical remarks

This contribution has presented a feasibility study of the fluid inerter for applications to earthquake engineering. The fluid inerter mechanical principle is based on a piston-cylinder device that generates a movement of a fluid through an external helical channel, thus producing rotational inertia of a fluid mass. In this contribution, a so-called Tuned Fluid Inerter (TFI) scheme has been elaborated, comprising a grounded fluid inerter and some linear restoring elements that can be realized, for instance, with low-damping rubber bearings. This novel TFI scheme has been combined with a classical isolation system made of friction pendulum (FP) isolators. It has been pointed out that, unlike mechanical variants of the inerter, the assumption of linear inerter is not accurate for describing the hysteretic features of the fluid inerter. Instead, a nonlinear damping contribution, mainly related to the pressure drops occurring in the helical channels, should be introduced. Therefore, a simplified scheme of the fluid inerter proposed in this paper comprises a linear inerter in parallel with a nonlinear dashpot element. The effect of such inherent nonlinear damping contribution of the fluid inerter in relationship to earthquake protection purposes has been analyzed and discussed in this paper.

An optimal design procedure based on random vibration theory has been presented, aimed at minimizing a specifically selected objective function under the assumption of base acceleration modeled as a stationary Kanai-Tajimi zero-mean Gaussian random process. The nonlinear terms of the FP isolators and of the fluid inerter are incorporated in the optimal design procedure through statistical linearization technique. The influence of the soil conditions (firm, medium and soft soil), of the design strategy (displacement-, acceleration-, or energy-oriented design procedure), and of the stiffness characteristics of the low-damping rubber bearings has been analyzed. Then, the seismic performance of the proposed FPS-TFI combined isolation system has been assessed in the time domain considering an ensemble of 100

ground-motion records belonging to the FEMA P695 database. This database comprises both far-field and near-fault earthquake events for the sake of generality. It has been found that the proposed FPS-TFI combined isolation system significantly reduces the isolators' displacement demand, as well as the interstory drift and absolute acceleration response of the superstructure. Moreover, the fluid inerter is better able to mitigate the seismic response under near-fault pulse-like events than the classical mechanical inerter, due to the inherent damping contribution.

Based on the encouraging results of this paper, further investigation should be directed towards the actual experimental behavior of large-scale fluid inerter devices to assess the suitability of the proposed TFI for practical earthquake protection purposes. To the authors' best knowledge, only small-scale prototypes of the fluid inerter have been tested so far, whereas more reasonable dimensions and more realistic load scenarios relevant to earthquake engineering applications should be considered in laboratory tests, which is the object of an ongoing research.

References

De Domenico, D., Deastra, P., Ricciardi, G., Sims, N.D., and D.J. Wagg. Novel fluid inerter based tuned mass dampers for optimised structural control of base-isolated buildings. *Journal of the Franklin Institute*, 356(14), 7626-7649, 2019a.

De Domenico, D., Gandelli, E., and V. Quaglini. Effective base isolation combining low-friction curved surface sliders and hysteretic gap dampers, *Soil Dyn Earthq Eng*, 130, 105989, 2020a.

De Domenico, D., and G. Ricciardi. Earthquake-resilient design of base isolated buildings with TMD at basement: Application to a case study, *Soil Dyn Earth Eng*, 113, 503-521, 2018a.

De Domenico, D., and G. Ricciardi. Optimal design and seismic performance of tuned mass damper inerter (TMDI) for structures with nonlinear base isolation systems, *Earth Eng Struct Dyn*, 47(12), 2539-2560, 2018b.

De Domenico, D., and G. Ricciardi., An enhanced base isolation system equipped with optimal Tuned Mass Damper Inerter (TMDI). *Earthq Eng Struct Dyn*, 47, 1169-1192, 2018c.

De Domenico, D., Ricciardi, G., and I. Takewaki. Design strategies of viscous dampers for seismic protection of building structures: a review. *Soil Dynamics and Earthquake Engineering*, 118, 144-165, 2019b.

De Domenico, D., Ricciardi, G., and R. Zhang. Optimal design and seismic performance of tuned fluid inerter applied to structures with friction pendulum isolators, *Soil Dyn Earthq Eng*, DOI: 10.1016/j.soildyn.2020.106099, 2020b.

Di Matteo, A., Masnata, C., and A. Pirrotta. Simplified analytical solution for the optimal design of Tuned Mass Damper Inerter for base isolated structures. *Mechanical Systems and Signal Processing*, 134, 106337, 2019.

Giaralis, A., and F. Petrini. Wind-induced vibration mitigation in tall buildings using the tuned mass-damper-inerter. *J Struct Eng*, 143(9), 04017127, 2017.

Giaralis, A., and A.A. Taflanidis. Optimal tuned mass-damper-inerter (TMDI) design for seismically excited MDOF structures with model uncertainties based on reliability criteria. *Structural Control and Health Monitoring*, 25(2), e2082, 2018.

Glover, A.R., Smith, M.C., Houghton, N.E., and P.J.G. Long. Force-controlling hydraulic device (International Patent Application No: PCT/GB2010/001491, 2009).

Gonzalez-Buelga, A., Lazar, I.F., Jiang, J.Z., Neild, S.A., and D.J. Inman. Assessing the effect of nonlinearities on the performance of a tuned inerter damper. *Struct Control Health Monit*, 24(3), e1879, 2017.

Hashimoto, T., Fujita, K., Tsuji, M., and I. Takewaki. Innovative base-isolated building with large mass-ratio TMD at basement for greater earthquake resilience, *Future Cities and Environment*, 1:9, 1-19, 2015.

Ikago, K. , Saito, K., and N. Inoue. Seismic control of single-degree-of-freedom structure using tuned viscous mass damper, *Earthq Eng Struct Dyn*, 41(3), 453-474, 2012.

Javidialesaadi, A., and N.E. Wierschem. An inerter-enhanced nonlinear energy sink. *Mechanical Systems and Signal Processing*, 129, 449-454, 2019.

Jiang, Y., Zhao, Z., Zhang, R., De Domenico, D., and C. Pan. Optimal design based on analytical solution for storage tank with inerter isolation system. *Soil Dyn Earthq Eng*, 129, 105924, 2020.

Lazar, I.F., Neild, S.A., and D.J. Wagg. Using an inerter-based device for structural vibration suppression. *Earthq Eng Struct Dyn*, 43, 1129-1147, 2014.

Lazar, I.F., Neild, S.A., and D.J. Wagg. Vibration suppression of cables using tuned inerter dampers. *Eng Struct*, 122: 62-71, 2016.

Luo, H., Zhang, R., Weng, D. Mitigation of liquid sloshing in storage tanks by using a hybrid control method. *Soil Dyn Earth Eng*, 90, 183-195, 2016.

Málaga-Chuquitaype, C., Menendez-Vicente, C., and R. Thiers-Moggia. Experimental and numerical assessment of the seismic response of steel structures with clutched inerters. *Soil Dyn Earth Eng*, 121, 200-211, 2019.

Pietrosanti, D., De Angelis, M., and M. Basili. Optimal design and performance evaluation of systems with Tuned Mass Damper Inerter (TMDI). *Earthq Eng Struct Dyn*, 46(8), 1367-1388, 2017.

Reggio, A., and M. De Angelis. Optimal energy-based seismic design of non-conventional Tuned Mass Damper (TMD) implemented via inter-story isolation. *Earth Eng Struct Dyn*, 44(10), 1623-1642, 2015.

Smith, M.C. Synthesis of mechanical networks: the inerter. *IEEE Transactions on Automatic Control*, 47(10), 1648-1662, 2002.

Smith, N., and D. Wagg. A fluid inerter with variable inertance properties, In: *6th European Conference on Structural Control (EACS2016)*, Sheffield, UK, 11-13 July 2016, paper no. 199.

Swift, S.J., Smith, M.C., Glover, A.R., Papageorgiou, C., Gartner, B., and N.E. Houghton. Design and modelling of a fluid inerter. *Int J Control* 86(11), 2035-2051, 2013.

Takewaki, I., Murakami, S., Fujita, K., Yoshitomi, S., and M. Tsuji. The 2011 off the Pacific coast of Tohoku earthquake and response of high-rise buildings under long-period ground motions, *Soil Dyn Earthq Eng*, 31(11), 1511–1528, 2011.

Takewaki, I., Murakami, S., Yoshitomi, S., and M. Tsuji. Fundamental mechanism of earthquake response reduction in building structures with inertial dampers. *Struct Control Health Monit*, 19, 590-608, 2012.

Taniguchi, T., Der Kiureghian, A., and M. Melkumyan. Effect of tuned mass damper on displacement demand of base-isolated structures, *Eng Struct*, 30, 3478-3488, 2008.

Wang, Q., Qiao, H. , De Domenico, D., Zhu, Z., and Z. Xie. Wind-induced response control of high-rise buildings using inerter-based vibration absorbers. *Applied Sciences*, 9(23), 5045, 2019.

Zargar, H., Ryan, K.L., and J.D. Marshall. Feasibility study of a gap damper to control seismic isolator displacements in extreme earthquakes. *Struct Control Health Monit*, 20(8), 1159–1175, 2013.

Zhao, Z., Zhang, R., Jiang, Y., and C. Pan. Seismic response mitigation of structures with a friction pendulum inerter system. *Engineering Structures*, 193, 110-120, 2019.